PNAS RESEARCH ARTICLE | DEVELOPMENTAL BIOLOGY

Human ERG oncoprotein represses *a Drosophila* LIM domain binding protein–coding gene *Chip*

Mahima Bharti[a], Anjali Bajpai[a,b], Umanshi Rautela[a,c], Nishat Manzar[a], Bushra Ateeq[a,b,1], and Pradip Sinha[a,b,1]

Edited by Hugo Bellen, Baylor College of Medicine, Houston, TX; received June 29, 2022; accepted October 24, 2022

Human ETS Related Gene, ERG, a master transcription factor, turns oncogenic upon its out-of-context activation in diverse developmental lineages. However, the mechanism underlying its lineage-specific activation of Notch (N), Wnt, or EZH2—three well-characterized oncogenic targets of ERG—remains elusive. We reasoned that deep homology in genetic tool kits might help uncover such elusive cancer mechanisms in *Drosophila*. By heterologous gain of human ERG in *Drosophila*, here we reveal *Chip,* which codes for a transcriptional coactivator, LIM-domain-binding (LDB) protein, as its novel target. ERG represses *Drosophila Chip* via its direct binding and, indirectly, via E(z)-mediated silencing of its promoter. Downregulation of *Chip* disrupts LIM–HD complex formed between Chip and Tailup (Tup)—a LIM–HD transcription factor—in the developing notum. A consequent activation of N-driven Wg signaling leads to notum-to-wing transdetermination. These fallouts of ERG gain are arrested upon a simultaneous gain of Chip, sequestration of Wg ligand, and, alternatively, loss of *N* signaling or *E(z)* activity. Finally, we show that the human *LDB1*, a homolog of *Drosophila Chip*, is repressed in ERG-positive prostate cancer cells. Besides identifying an elusive target of human ERG, our study unravels an underpinning of its lineage-specific carcinogenesis.

ERG | Chip | LDB1 | Cancer | Wnt

Significance

Nuclear targets of oncoproteins help decipher cancer mechanisms. Targets of human ERG oncoprotein identified so far have not helped unravel its lineage-specific carcinogenesis. Here, we reveal an alternative strategy to discover ERG targets via its heterologous gain in *Drosophila* and display *Chip*, a LIM-domain-coding gene, as its target. ERG-mediated *Chip* repression induces out-of-context Wg signaling in the notum (thorax) primordium leading to notum-to-wing transdetermination. Further, ERG induces carcinogenesis in the notum in combination with the loss of Lgl tumor suppressor. Remarkably, ERG-positive prostate cancer cells, too, show repression of *LDB1*, a human homolog of *Drosophila Chip*. Our results present a strategy to discover functionally relevant oncoprotein targets and unravel essential cancer mechanisms in *Drosophila*.

Evolutionary conservation of genetic tool kits such as cellular signaling pathways and homeotic selectors regulating cell lineages, fates, and pattern formations in animals from distant phylogenies reveals deep homology (1). Apart from these well-known genetic tool kits, LIM–homeodomain (LIM–HD) transcription factors are also conserved across the animal kingdom (2). Examples of this class of LIM–HD transcription factors include Tailup (Tup) and Apterous (Ap) in *Drosophila;* their mammalian homologs being Islet and LIM–homeobox, respectively [for reviews, see ref. 3]. LIM–HD transcription factors are activated by forming tetrameric complexes with a transcription cofactor, LIM-domain-binding (LDB) protein: Chip, in *Drosophila* (4, 5) and its homolog, LIM Domain Binding, LDB, in mammals [reviewed in ref. 6]. Conservation of LIM–HD complexes across phylogeny (2) also underscores the pervasive nature of deep homology in developmental lineage specification and pattern formation across insects (7) to mammals (8, 9).

During mammalian development, expression of ERG (ETS-Related Gene) master transcription factor is seen in endothelial cells and organs of mesodermal lineage: for instance, developing kidney, urogenital tract, hematopoietic cells, cartilage, and neural crest cells (10, 11). In adults, ERG expression is seen in the cells of endothelial (10, 11) but not in those of epithelial lineages, including the prostatic epithelium (12). Out-of-context ERG activations via chromosomal translocations and fusion with promoters of active genes in select cell lineages trigger carcinogenesis. Prostate cancer (13, 14), Ewing sarcoma (15), or acute myeloid leukemia (16) are some of the exemplars of the extreme diversity of ERG-induced lineage-specific cancers. ERG targets have so far been identified by genome-wide screening of its binding. In prostate cancer, for instance, activated ERG (13) partners with HOXB13 and FOXA1 for binding to its targets; subsets of these ERG targets show enrichment of Notch (N) signaling pathway members (17). ERG-induced prostate cancer also display upregulation of Wnt ligands (18) and EZH2, a member of the Polycomb group complex (19), besides DLX1, a homeobox transcription factor (20). A major hallmark of ERG-induced cancers is phenotypic plasticity, suggesting their cell fate reversals *en route* to their metastatic progression [for review, see ref. 21]. However, despite identifying these ERG targets in diverse cancers (14), underpinnings of its lineage-specific carcinogeneses remain elusive.

It has long been recognized that heterologous expression of mammalian transcription factors in *Drosophila* identifies targets that display deep homology. Seminal reports on homeotic transformations in *Drosophila* following heterologous expression of mammalian Hox-2.2 (22) or Pax6 master transcription factors (23) revealed conserved downstream targets. Like Hox-2.2 or Pax6, the ERG master transcription factor displays an ancient

Author contributions: M.B., A.B., B.A., and P.S. designed research; M.B. and N.M. performed research; M.B. and U.R. contributed new reagents/analytic tools; M.B., A.B., and N.M. analyzed data; B.A. and P.S. conceptualization; and M.B., A.B., B.A., and P.S. wrote the paper.

The authors declare no competing interest.

This article is a PNAS Direct Submission.

[1]To whom correspondence may be addressed. Email: bushra@iitk.ac.in or pradips@iitk.ac.in.

This article contains supporting information online at https://www.pnas.org/lookup/suppl/doi:10.1073/pnas.2211189119/-/DCSupplemental.

Published January 3, 2023.

metazoan origin (24), and its evolution is marked by the conservation of its DNA-binding ETS and PNT domains [for review, see ref. 25]. We thus hypothesized that a gain of human ERG master transcription factor in *Drosophila* would uncover its yet elusive targets, particularly those which underpin its capacities to induce lineage-specific carcinogenesis.

Here, we have expressed ERG oncoprotein in *Drosophila* developing appendages and revealed the repression of its novel target, *Chip*. Further, reminiscent of that seen in prostate cancer (19), heterologous ERG binds to *E(z),* the *Drosophila* homolog of mammalian *EZH2*. ERG-induced E(z) epigenetically silences *Chip* transcription, disrupting the Chip–Tup, LIM–HD complex. A consequent reactivation of N-triggered Wg synthesis in the posterior notum culminates in notum-to-wing transdetermination. Further, upon losing a tumor suppressor, like Lgl, ERG-expressing notal cells display cooperative carcinogenesis via N-Wg signaling. Finally, we show that ERG-positive prostate cancer cells display downregulation of *LDB1,* a human homolog of *Drosophila Chip*. These results present a strategy to identify human oncoprotein targets and decipher cancer mechanisms in *Drosophila.*

Results

Heterologous ERG Induces Notum-to-Wing Transdetermination by Triggering Ectopic N-Wg Signaling. The proximal and distal domains of the developing wing imaginal disc of *Drosophila* give rise to the adult thorax (notum) and wing proper, which are held together by a hinge domain. Ap, LIM–HD, and Engrailed (En), homeobox, transcription factors, respectively, specify the dorsal (D) and posterior (P) compartments of the wing primordium [Fig. 1*A*, for review, see ref. 26]. DV and AP boundaries of the developing wing double up as signaling centers regulating its anisotropic growth by sending out Wg (a Wnt) and Dpp (a BMP) morphogens, respectively [for recent articles, see refs. 27–29]. The presumptive adult wing is marked by a POU-domain protein, Nubbin [Nub, Fig. 1*B*; (30)], a target of Wg [Fig. 1*C*; (30–33)]. Nub also marks the inner of the two epithelial folds of the presumptive wing hinge region [blue arrowhead, Fig. 1*B*, also see refs. 31].

To examine the fallout of a heterologous gain of ERG oncoprotein, we drove its expression in the larval wing imaginal discs under four different Gal4 drivers individually. These were *en-Gal4* [*en>GFP,* Fig. 1*A*, (35)], *vg-Gal* [boundary enhancer-BE, *vg>GFP* Fig. 1*D*, (36)], *ci-Gal4* [*ci>GFP*, *SI Appendix*, Fig. S1*A*, (37)], and *dpp-Gal4* [*dpp>GFP*, *SI Appendix*, Fig S1*C*, (38)]. Gain of ERG under *vg-Gal4* (star, Fig. 1*E*) or *en-Gal4* driver (stars, Fig. 1 *F–I*) induced a striking fallout, namely, ectopic expression of Nub in the presumptive notum, revealing a notum-to-wing cell fate switch or transdetermination [for review, see ref. 39]. In extreme scenarios, the transdetermined wing primordium (star, Fig. 1*G*) outgrew its endogenous counterpart. More than one transdetermined wing primordia were infrequently seen in *en>ERG* notum (stars, Fig. 1 *H* and *I*). Frequencies of transdetermined wings progressively declined in the order of the Gal4 used: namely, *en-Gal4*, *vg-Gal4, dpp-Gal4,* and *ci-Gal4* (Fig. 1*J*). Notably, plotting the domains of these Gal4 drivers revealed a shared feature: their expression within or abutting the presumptive posterior notum of the wing imaginal disc wherein out-of-context Nub was induced (yellow stippled dots, Fig. 1*K*). Thus, ERG-gain under these Gal4 drivers induced ectopic Nub in only the posterior notum, even while their expressions extended far beyond this domain. The posterior notum, therefore, displayed hallmarks of a hotspot: that is, a sensitive zone for cell fate switch as seen during regeneration of the leg (40) or upon gain of Eyeless (Ey) master transcription factor in the wing, leg, eye, and haltere imaginal discs (23, 41).

Wg expression is seen in an anterior ventral wedge (42) in the distal wing imaginal disc of the early second larval instar (33). These Wg-expressing cells represent the progenitors of the future adult wing (42) and are marked by expression of Nub and, Vestigial, Vg (33), the latter being a wing cell fate selector (43). Subsequently, during third larval instar, growth and patterning of the wing primordium are driven by Wg morphogen synthesized and secreted from its DV signaling center (28, 29, 33, 42, 44). -The third larval instar wing imaginal disc, therefore, Wg displays its characteristic, spatially restricted morphogen signaling from the DV boundary, which drives wing growth and patterning (27–29, 33).

N regulates Wg during second phase of its wing growth-promoting role (27–29, 44–46). We noted that the gain of a constitutively active N receptor, N^{intra} (47), too, induced a notum-to-wing cell fate switch (star in Fig. 1*L*), reminiscent of that seen upon the gain of ERG (Fig. 1 *E–I*). Conversely, coexpression of ERG and a dominant-negative form of N, namely, N^{DN} (48), or that of its downstream target, Mastermind, Mam^{DN} (49), extinguished wing transdetermination in the posterior notum (blue star, Fig. 1 *M* and *N*). Further, coexpression of ERG and a membrane-anchored Frizzled (Fz) receptor, GPI-dFz2—which tethers Wg ligand to the membrane arresting its signal transduction (50)—suppressed wing transdetermination (blue star, Fig. 1 *O* and *P*). Finally, ERG gain in the haltere induced metanotum-to-capitellum transdetermination (Fig. 1 *Q–S*), which is anticipated given that these two dorsal appendages, the wing and haltere, share common developmental ground plan and genetic tool kits (34).

ERG-Induced Wg in the Notum Displays Both Its Early Wing-Specifying and Late Growth-Promoting Roles. ERG-expressing second instar larval wing imaginal disc, however, did not display notum-to-wing transdetermination, as revealed by the absence of Nub expression (blue star, *en>ERG*, Fig. 2*A*), while at this stage, the endogenous wing primordium displayed its characteristic expression (arrow, *en>ERG,* Fig. 2*A*). Subsequently, in a mid-third instar *vg>ERG* wing imaginal disc, we noticed induction of Nub (31–33) at a far posterior margin of its notum (star, Fig. 2 *B* and *B'*). Induction of Nub expression in these cells of notum by ERG was cell-autonomous (yellow arrowheads in Fig. 2 *B'* and *B"* and XZ optical section in Fig. 2*B'*) as well as non-cell autonomous (red arrowhead in Fig. 2 *B'* and *B"* and XZ section in Fig. 2*B'*). These characteristics were further quantified by their fluorescence intensities (Fig. 2*C*) and colocalization (Fig. 2*D*, see *SI Appendix, Methods*). These results suggest that Wg induced in ERG-expressing cells of the posterior notum is secreted. Indeed, ERG-expressing somatic clones in the posterior notum displayed cell-autonomous (yellow arrowhead, broken line, Fig. 2 *E* and *E"*) and extensive non-cell-autonomous notum-to-wing cell fate switches (red arrowhead, Nub, Fig. 2 *E* and *E"*), as can be anticipated from their secretion of the long-range Wg morphogen (51). Moreover, we also noticed cell-autonomous and non-cell-autonomous Wg expressions, respectively, within (broken line, Fig. 2 *F'* and *F"*) and around (arrow, Fig. 2 *F'* and *F"*) the ERG-expressing clone in the posterior notum.

Starting mid-third larval instar stage, *en>ERG* wing imaginal discs displayed Wg expression in the notum, straddling the anterior (A) and posterior (P) compartment boundary (broken line, Fig. 2*G*). In older third larval wing imaginal discs, cell-autonomous and non-cell-autonomous Wg expressions in transdetermined wing primordia were more pronounced (Fig. 2 *H* and *I*). Finally, we also noticed instances where Wg expression in the transdetermined wing matched its endogenous counterpart (Fig. 2 *J* and *J'*). In ERG-expressing adult thorax, we noticed amorphic wing tissue growth

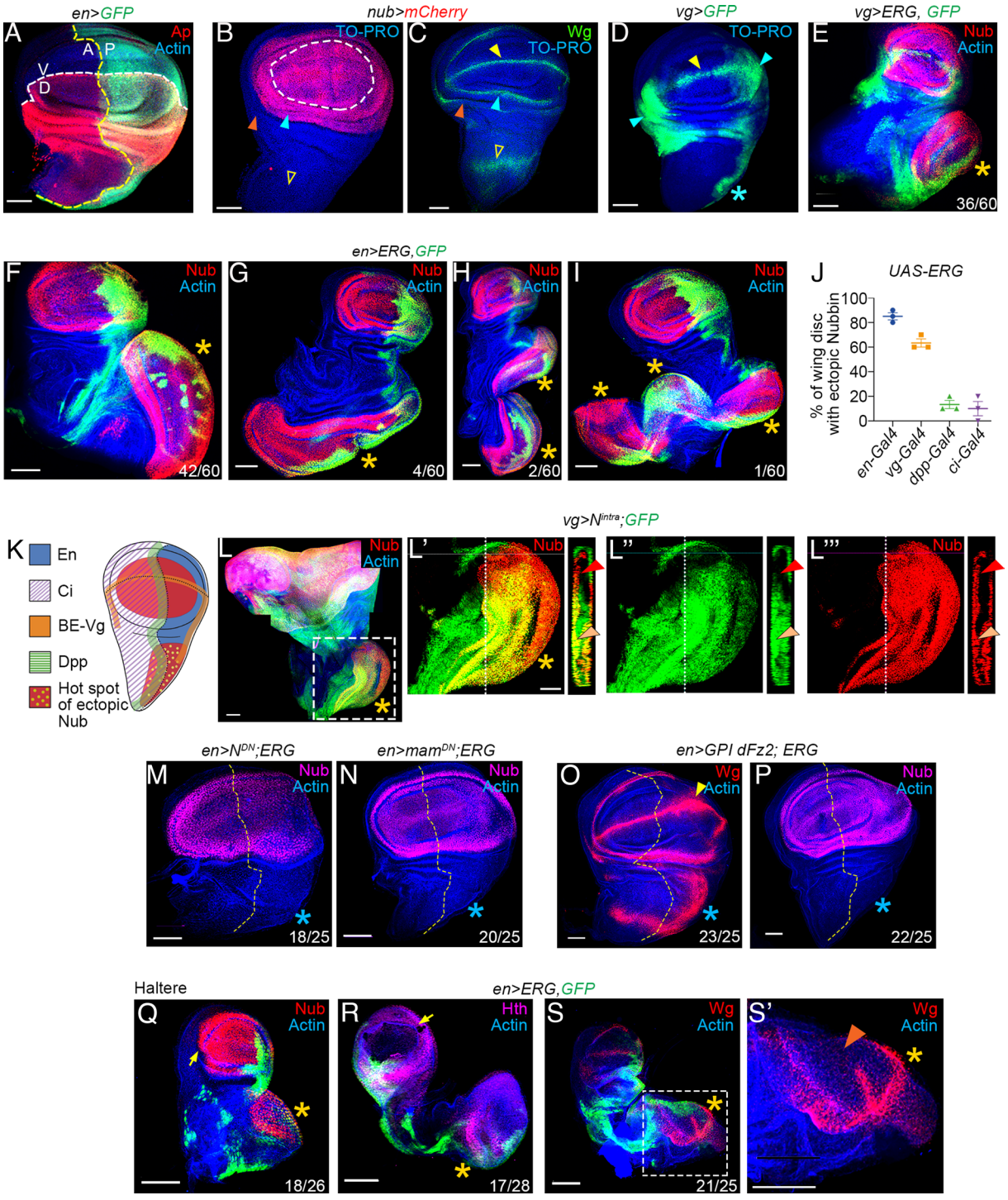

Fig. 1. Human ERG oncoprotein induces notum-to-wing transdetermination in *Drosophila*. (*A–C*) Apterous (red, Ap, *A*) and *en>GFP* (green, *A*), respectively, mark the dorsal (D) and posterior (P) compartments of the wing imaginal disc. Yellow and white broken lines mark the AP and DV compartment boundaries, respectively (*A*). Nub (red, *nub>mCherry*) expression marks the presumptive adult wing pouch (broken line, *B*) and the inner (blue arrowhead, *B*), but not the outer epithelial fold (orange arrowhead, *B*) of the hinge, and notum (open arrowhead). Wg expression (green) is seen in the DV boundary (yellow arrowhead, *C*) in both the inner and outer rings of the hinge domain (orange and blue arrowheads, *C*) and the notum (open arrowhead). Distal (wing pouch) is up, and proximal (notum) is down in this and all subsequent images. (*D*) Domain of expression of the *vg-Gal4* driver (*vg>GFP*, green, *D*) on the DV boundary (yellow arrowhead), hinge (blue arrowheads), and in a trail of cells till the edge of the posterior notum (star). (*E* and *F*) ERG expression under *vg-Gal4* (*vg>ERG, GFP,* green, *E*) or *en-Gal4* (*en>ERG, GFP,* green, *F*) drivers induce ectopic Nub in the notum; yellow star here (stars, *E* and *F*) and elsewhere marks the notum-to-wing transdetermination. (*G–I*) Examples of *en-Gal4>ERG* wing imaginal disc displaying one (star, *G*), two (stars, *H*) or three (stars, *I*) transdetermined wing primordia in the notum (Nub, red, *G–I*). (*J* and *K*) Frequency of notum-to-wing transdetermination upon the gain of ERG under *en-Gal4, vg-Gal4, dpp-Gal4,* or *ci-Gal4* driver (*J*). Schematic display of domains of these Gal4 expressions revealing their overlap on a hot spot (yellow stippled dots in a red zone) of wing transdetermination in the posterior notum (*K*). (*L*) Constitutive gain of N, (*vg>N^{intra}, GFP*, green). The boxed area in (*L*) is shown at higher magnification in (*L'–L'''*). XZ optical section further reveals autonomous (orange arrowheads) and non-autonomous (red arrowheads) gain of Nub (red, *L'–L'''*). (*M–P*) Co-expression of ERG with a dominant-negative form of N (blue star, *en>ERG; N^{DN}*, *M*) or its downstream effector Mam (blue star, *en>ERG; mam^{DN}*, *N*) arrest wing transdetermination in the notum (blue star). Coexpression of a membrane-tethered receptor, *GPI-dFz2* with *ERG* (*en>ERG; GPI-dFz2*) sequesters the Wg ligand in the DV signaling center (yellow arrowhead, *O*) and the posterior notum (blue star, *O*), with accompanying loss of notum-to-wing transdetermination (loss of Nub, blue star, *P*). (*Q–S*) Haltere imaginal disc displaying metanotum-to-capitellum transdetermination (Nub, star, *en>ERG*, *Q*). Also, note the proximal (Hth, *R*) and distal patterning in the transdetermined haltere (star, Wg, *S*). The boxed area in (*S*) is displayed at higher magnification in the right panel to reveal the absence of Wg in the posterior DV margin of the transdetermined capitellum, a characteristic of endogenous haltere primordium [orange arrowhead, *S'*, (34)]. Scale bars, 50 μm; N=number of transdetermined wing primordia/total number.

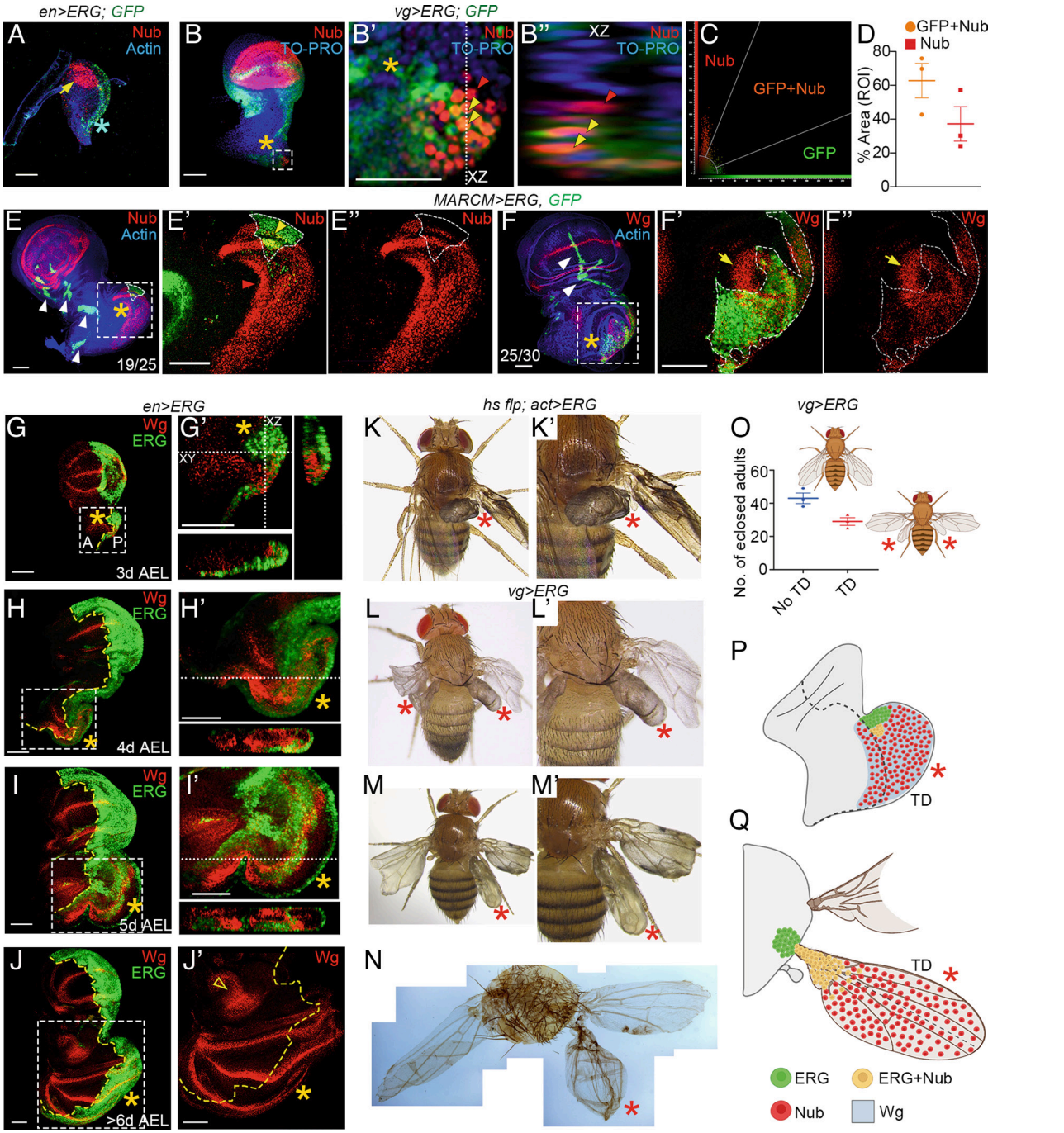

Fig. 2. ERG-induced Wg specifies wing cell fate and promotes wing growth in the posterior notum. (*A*) An ERG-expressing, second instar wing imaginal disc (*en>ERG; GFP*, green): Nub (arrow) marks the presumptive wing; Nub expression is not seen in the developing notum (blue star), despite ERG gain at this stage (for comparison, see Fig. 1 *F* and *G*). (*B–D*) Mid-third instar *vg>ERG* wing imaginal disc displaying an early sign of notum-to-wing transdetermination in the posterior notum (star, Nub, 2B). The boxed area in (*B*) is shown at higher magnification in (*B′*). An XZ optical section along the dotted line in *B′* is shown in *B″*. Note the cell-autonomous (yellow arrowheads *B′*, *B″*) notum-to-wing cell fate switch as seen from expression of both the ERG (GFP, green) and Nub (red). Also, note the non-cell autonomous Nub expression (red arrowhead, *B′*, *B″*) in a cell neighboring the ERG-expressing cells (yellow arrowhead, orange fluorescence *B′*, *B″*). Fluorescence intensities in (*B′*) is also shown in a scatter plot (*C*). A substantial fraction cells display non-cell autonomous gain of Nub in this region of interest (dot plot, red, *D*). (*E* and *F*) Mosaic wing epithelium with ERG-expressing clones (*MARCM>ERG, GFP*, green, *E* and *F*). A broken line outlines the clonal area in both. A magnified view of the boxed area from (*E*) is shown in (*E′*) to reveal its cell-autonomous (yellow arrowhead, *E′*) and largely non-cell-autonomous (red arrowhead, *E′*) notum-to-wing transdetermination (red, Nub, *E′*). The red channel (Nub, *E′*) is shown separately in (*E″*). A magnified view of the boxed area of (*F*), is shown in (*F′*). Note the non-cell-autonomous (arrow, *F′*, *F″*) and cell-autonomous (within the broken line, *F′*, *F″*) expression of Wg (red) in fixed preparation of mosaic wing imaginal disc. Clones formed outside the posterior notum do not induce Nub (white arrowheads, *E* and *F*). (*G–J*) Cell-autonomous and non-cell-autonomous induction of Wg (red) in ERG-expressing nota of *en>ERG* wing imaginal discs. Boxed areas of 3 to 6-d-old, third instar larval wing imaginal discs (*en>ERG*; *G–J*) are shown at higher magnification in (*G′–J′*). XZ and XY (*G*) or only XY (*H* and *I*) optical sections are also displayed. Open arrowhead (*J′*) marks the endogenous notum-specific Wg expression. (*K–N*) Adults eclosed from the indicated genotypes display a range of notum-to-wing transdetermination ranging from amorphous wing growth (*K* and *L*) to near completely patterned wing (*M* and *N*). Higher magnifications are shown on the right (*K′–M′*). (*O*) The number of *vg>ERG* adults with notum-to-wing transdetermination (TD) or without (No TD). (*P* and *Q*) Schematic interpretation of ERG-induced notum-to-wing transdetermination (TD) in the notum of wing imaginal disc (*P*) and adult mesothorax (*Q*). Color scheme of different cell types and Wg gradient are shown at the bottom. Scale bar, 50 μm.

(stars, Fig. 2 *K* and *L*) to transdetermination into wing proper that appeared patterned (stars, Fig. 2 *M* and *N*), like their endogenous counterparts. Overall, about two-thirds of the eclosed *vg>ERG* adults displayed notum-to-wing transdetermination (Fig. 2*O*). Further, transdetermined wing primordia showed growth along their AP, DV, and PD axes (*SI Appendix*, Fig. S1 *E–H*), suggesting their anisotropic growth via AP and DV morphogen-signaling centers, much like their endogenous counterpart (27, 29).

Our results reveal that ERG-triggered Wg induces both cell-autonomous and non-cell-autonomous notum-to-wing cell fate switches (Fig. 2*P*). A near-perfect patterning of the transdetermined wing, although infrequent, suggests the development of DV and AP signaling centers in these transdetermined wings by mechanism(s) that can only be speculated based on the emergent understanding of the growth and patterning in the endogenous wing primordium [(27–29, 33, 42, 44), see *Discussion*].

Heterologous ERG and Its *Drosophila* Ortholog, Ets21C, Both Target *Chip* for Repression at Conserved ERG-Binding Sites (EBS). LIM–HD protein complexes maintain developmental domain-specific cellular signaling and cell fate during the development of *Drosophila* appendages (5, 52, 53). For instance, Chip–Tup (52, 54) and Chip–Ap (4, 5) are, respectively, active in the proximal (notum) and distal (wing) domains of the wing imaginal disc, maintaining their respective cell fates. Therefore, it is plausible that the loss of Chip, Tup, or both underlies the notum-to-wing cell fate switch seen upon ERG gain.

We noticed a transcriptional downregulation of *Chip* in *en>ERG* wing imaginal discs (Fig. 3 *A–C*). Therefore, ERG-induced notum-to-wing transdetermination is likely linked to Chip loss. In agreement, we noticed that compromising Chip activity by expressing a dominant-negative form of Chip, Chip$^{\Delta oid}$—which partially lacks its other interacting domain, OID (55)—in somatic clones (Fig. 3*D*) or under the *en-Gal4* driver (Fig. 3*E* and *SI Appendix*, Fig. S4*C*) induced ectopic Nub expression in the notum. We also recovered *vg-Gal4>ChipΔ^{oid}* adults, which showed *de novo* wing development in the thorax (Fig. 3*F*). Further, knockdown of *Chip* (*en>Chip-RNAi*, Fig. 3*G*), too, phenocopied ERG gain (see Figs. 1 and 2). Conversely, a simultaneous gain of Chip and ERG abrogated de novo Nub (Fig. 3*H*) or Wg (Fig. 3*I*) expressions in the notum. These results reveal that ERG-induced notum-to-wing transdetermination entails a downregulation of *Chip*.

ERG-mediated repression of *Chip* is also likely to affect Chip–Ap tetramers formed in the dorsal wing pouch (4, 5). We noted that the *ap* expression revealed by its *ap-lacZ* reporter in the dorsal wing primordium was not perturbed by ERG gain (*SI Appendix*, Fig. S2*A*). In the notum, *ap* displays a non-uniform pattern of expression (*ap-lacZ*, *SI Appendix*, Fig. S2 *B–D*). We reasoned that ERG-induced *Chip* downregulation—and consequently, loss of Chip–Ap tetramers in the dorsal wing—might compromise Ap activity, which likely culminates in the development of de novo Ap^{+}/Ap^{-} boundary: that is, DV signaling center (57, 58). Surprisingly, a ubiquitous gain of ERG (Fig. 1) or loss of *Chip* (Fig. 3) under different Gal4 drivers did not display signs of ectopic DV signaling center development in the endogenous wing primordium. By contrast, ERG-expressing somatic clones induced ectopic DV signaling centers in only select spatial domain of dorsal wing primordium (*SI Appendix*, Fig. S2 *E–F*) while *Chip* loss-of-function clones invariably induce ectopic DV boundaries in the dorsal wing pouch (59). Thus, ERG-expressing clones

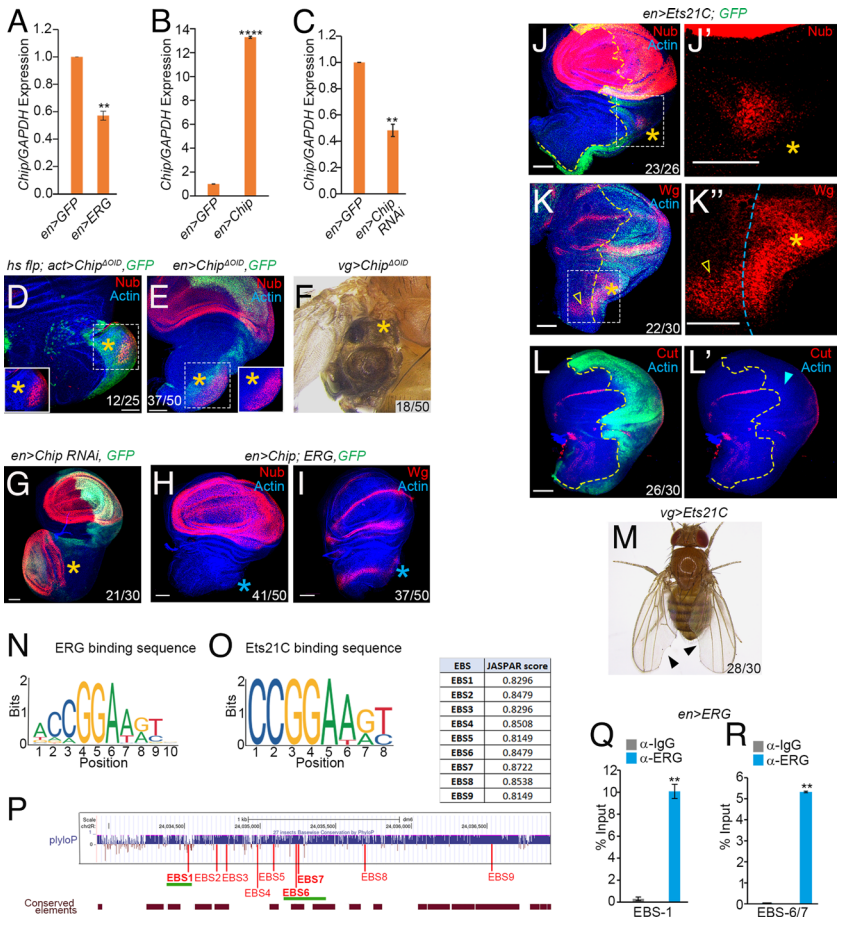

Fig. 3. Both ERG and its *Drosophila* ortholog, Ets21C, target *Chip*. (*A–C*) Quantification of *Chip* RNA (RT-qPCR) from wing epithelia expressing ERG (*en>ERG*, *A*), *Chip* (*en>Chip, B*) or displaying knockdown of *Chip* (*en>Chip-RNAi*, *C*); fold changes in *Chip* RNA are displayed as ratios to that of internal control, *GAPDH*. **P<0.005. (*D–I*) Clonal expression of a dominant-negative form of Chip (*ChipΔ^{oid}*, GFP, *D*) or its expression under an *en-Gal4* driver (*en>ChipΔ^{oid}, GFP*, *E*) displayed notum-to-wing transdetermination (star, Nub, *D* and *E*; *Insets* display only the Nub channel). *vg>ChipΔ^{oid}* adult displaying ectopic but amorphous wing development in the adult thorax (star, *F*). *en>Chip-RNAi* displaying ectopic Nub in notum (star, Nub, *G*). Coexpression ERG and Chip extinguished notum-to-wing transdetermination as seen from the absence of Nub (blue star, *en>Chip, ERG*, *H*). These wing imaginal discs also failed to display ectopic Wg in notum (blue star, *en>Chip, ERG*, *I*). (*J–M*) Gain of Ets21C, a *Drosophila* ortholog of mammalian ERG (*en>Ets21C, GFP*, *J–L*). Magnified boxed area of (*J* and *K*) in the posterior notum reveals its incipient gain of Nub (star, *J'*) and elevated Wg (*K'*); open arrowhead marks the endogenous notum-specific strip of Wg (*K* and *K'*, also see Fig. 1*C*). These Ets21C-expressing wing imaginal discs display suppression of an N target, Cut, in the posterior DV margin (*L* and *L'*, blue arrowhead in *L'*). Most *vg>Ets21C* animals eclosed as adults with a characteristic notched-wing phenotype (arrowheads, *M*). (*N–P*) Consensus DNA-binding sequences of ERG (*N*) and Ets21C (*O*) as predicted by JASPAR (56). A schematic representation of evolutionary conservation of −3.0kb cis-regulatory module (CRM) upstream of *Chip* transcription start site (TSS) across 27 insect species. Approximate positions of the predicted ERG/Ets21C-binding sites (EBSs) are marked by nine red vertical bars, while the bottom brown horizontal bars displayed highly conserved elements calculated by phastCons. Two horizontal green lines mark the regions, which were further tested for physical binding of ERG by performing ChIP-qPCR. The inset table displays individual conservation scores of these nine EBSs, as generated by JASPAR. (*Q* and *R*) Enrichment of ERG binding to EBS1 and EBS6/7 assayed by ChIP-qPCR from *en>ERG* wing imaginal discs using an anti-ERG antibody. **P < 0.001. Scale bar, 50μm, N= number of transdetermined wing primordia/total number.

might cause a partial and incomplete depletion of *Chip* levels. Alternatively, it is also plausible that the Chip–Tup complex in the notum is more sensitive to ERG gain than Chip–Ap.

Ets21C [synonym Ets6, (60)] is a *Drosophila* ortholog of ERG that displays 86% and 26% identity of its ETS- and PNT-domains with those of its human counterpart, respectively (60–63). Ets21C expression is triggered during regeneration and tumorigenesis (64, 65), while its gain in oncogenically targeted cells induces cooperative carcinogenesis in *Drosophila* (62, 63, 65, 66). We noted that ectopic gain of Ets21C induced Nub and Wg expressions in the posterior notum (Fig. 3 *J–K*), albeit far less strikingly than that seen upon ERG gain (Figs. 1 and 2) or *Chip* loss (Fig. 3 *A–F*). Moreover, a gain of Ets21C under *en-Gal4* driver displayed suppression of N target, Cut (Fig. 3*L*) at the wing primordium's DV boundary, culminating in characteristic notched wing phenotypes in adult flies (Fig. 3*M*).

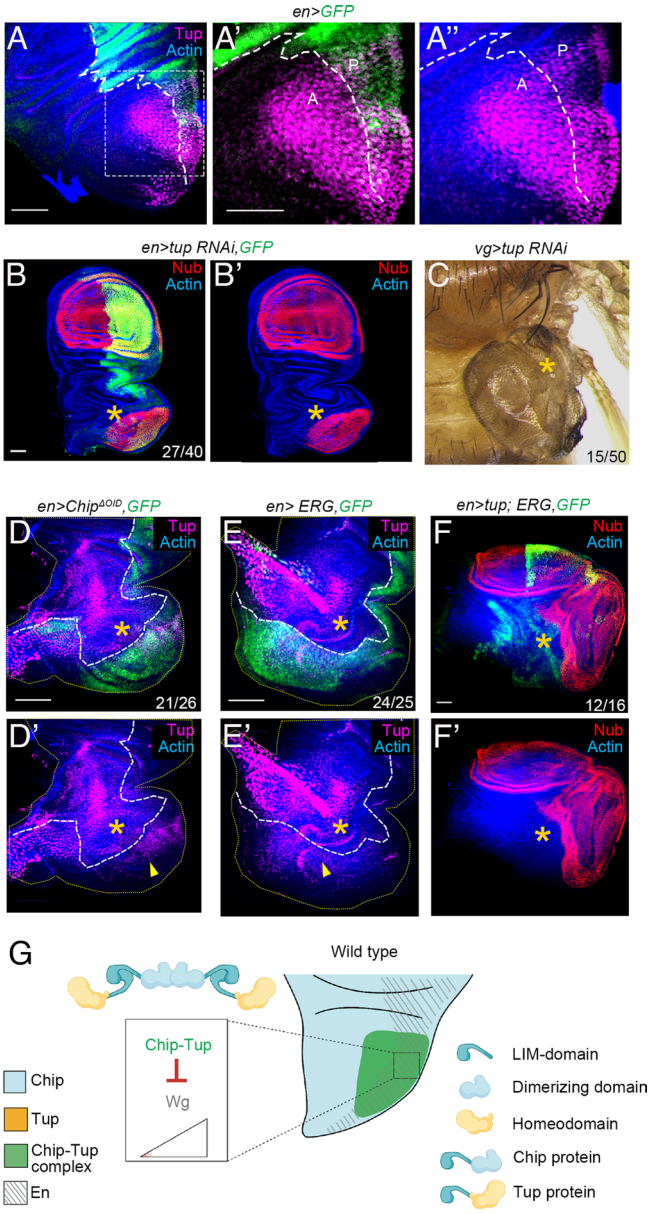

Fig. 4. Knockdown of Tup, a LIM–HD binding partner of Chip, induces notum-to-wing transdetermination. (*A–A''*) Domain of expression of Tup (magenta) in the notum of the third instar wing imaginal disc (*A*); broken line marks the AP compartment boundary (*en>GFP;* green, *A*). Boxed area of (*A*) is shown at higher magnification in (*A'* and *A''*). (*B* and *C*) Knockdown of *tup* in wing imaginal disc induced notum-to-wing transdetermination (star, Nub, *en>tup-RNAi; B* and *B'*), while the adult mesothorax displayed amorphous wing growth (star, a *vg>tup-RNAi, C*). (*D–F*) Loss of *Chip* (green, *en>Chip*Δ^{oid}*, GFP, D*) or gain of ERG (green, *en>ERG, GFP, E*) fails to suppress Tup in the transdetermined wing (star, *D'* and *E'*). A simultaneous gain of *tup* and ERG, too, fails to suppress notum-to-wing transdetermination (star, *en>tup; ERG, F* and *F'*; for comparison, see Fig. 3 *H* and *I*). (*G*) Schematic representation of Chip–Tup complex-mediated repression of wing cell fate in the posterior notum. Scale bar, 50 μm, N= number of transdetermined wing primordia/total number.

We further noted that the DNA-binding sequence of ERG (Fig. 3*N*) and Ets21C (Fig. 3*O*) are highly conserved [CCGGAA (Fig. 3 *N* and *O*)]. To examine if *Chip* is a transcriptional target of ERG and Ets21C, we examined a –3.0kb region upstream of its TSS (transcription start site) for putative Ets21C/ERG binding site (EBS). Such an upstream region of *Chip* may serve as its CRM (cis-regulatory module). We found nine putative Ets21C-binding sites in this –3.0-kb CRM of *Chip*; eight of these were putative ERG binding sites, (*SI Appendix*, Fig. S2*C*). Next, we looked for conservation of the EBS containing CRM of *Chip* across different insect species. Two standard bioinformatics analysis methods were used for the estimation of evolutionary conservation: phyloP (44, 67) and phastCons [(68), see *SI Appendix, Methods*] across 27 insect species available at the UCSC genome browser portal. We noticed positive phyloP scores for most nucleotides in this CRM of *Chip* (*SI Appendix*, Fig. S3*A*). Likewise, phastCons analysis, too, revealed stretches of nucleotide runs with a positive score (*SI Appendix*, Fig. S3*A*), indicating their conservation across all 27 insect species. We noted that six of the predicted EBSs were located within "Conserved Elements" based on phastCons scores (Fig. 3*P* and *SI Appendix*, Fig. S3*B*). Finally, chromatin immunoprecipitation (ChIP) of *en>ERG* imaginal discs confirmed the binding of ERG on three (EBS1, EBS6, and EBS7) of the nine EBSs in the CRM of *Chip* (Fig. 3 *Q* and *R*).

The Spatial Domain of Tup Expression in the Posterior Notum Underpins Lineage-Specific Fallouts of ERG Gain. While the expression of *Chip* is ubiquitous throughout the wing imaginal discs (69), its LIM–HD-binding partner, Tup, is selectively expressed in the notum of the wing primordium [Fig. 4*A*, see refs. 54], that largely overlaps with the domain of expression of the posterior cell fate-specifying selector, En (also see Fig. 1*A*). Consequently, the Chip–Tup tetrameric complex remains restricted to the Tup-expressing cell of the notum. Not surprisingly, *tup* knockdown induced selective notum-to-wing transdetermination in the Tup-expressing cells of the notum (Nub, Fig. 4 *B* and *C*; Cut, *SI Appendix*, Fig. S4*D*, also see Fig. 1 *E* and *F*"), reminiscent of that seen upon ERG-induced *Chip* loss. Loss of Tup in the distal wing did not down-regulate N-Wg signaling (*SI Appendix*, Fig. S4 *D* and *D*")—unlike that seen upon loss of Chip (Fig. 3 *D–G*)—which is consistent with the fact that the Chip–Tup complex is formed only in the posterior notum. Further, neither Chip loss (Fig. 4*D*) nor ERG gain (Fig. 4*E*) repressed Tup expression. Finally, *tup* gain—unlike that of Chip (see Fig. 3 *H* and *I*)—failed to arrest ERG-induced notum-to-wing transdetermination (Fig. 4*F*). These results reveal that spatial regulation of Tup (Fig. 4*G*) dictates the fallout of heterologous ERG, although it is not a direct target of repression by the latter.

ERG-Induced E(z) Epigenetically Silences *Chip*. By a direct binding on *EZH2* (19), ERG upregulates its expression in different cancers [for review, see ref. 70]. In ERG-expressing wing epithelium, *E(z)* (71), a *Drosophila* homolog of mammalian *EZH2*, was seen upregulated (*en>ERG*, Fig. 5*A*). Further, in a –3.0kb CRM upstream of *E(z)* TSS, we notice three putative Ets21C-binding sites, two of which were also putative ERG binding sites (Fig. 5*B* and *SI Appendix*, Fig. S5*C*). Notably, this *E(z)* CRM was conserved across 27 insect species (*SI Appendix*, Fig. S5 *A* and *B*). Finally, we confirmed the binding of ERG on

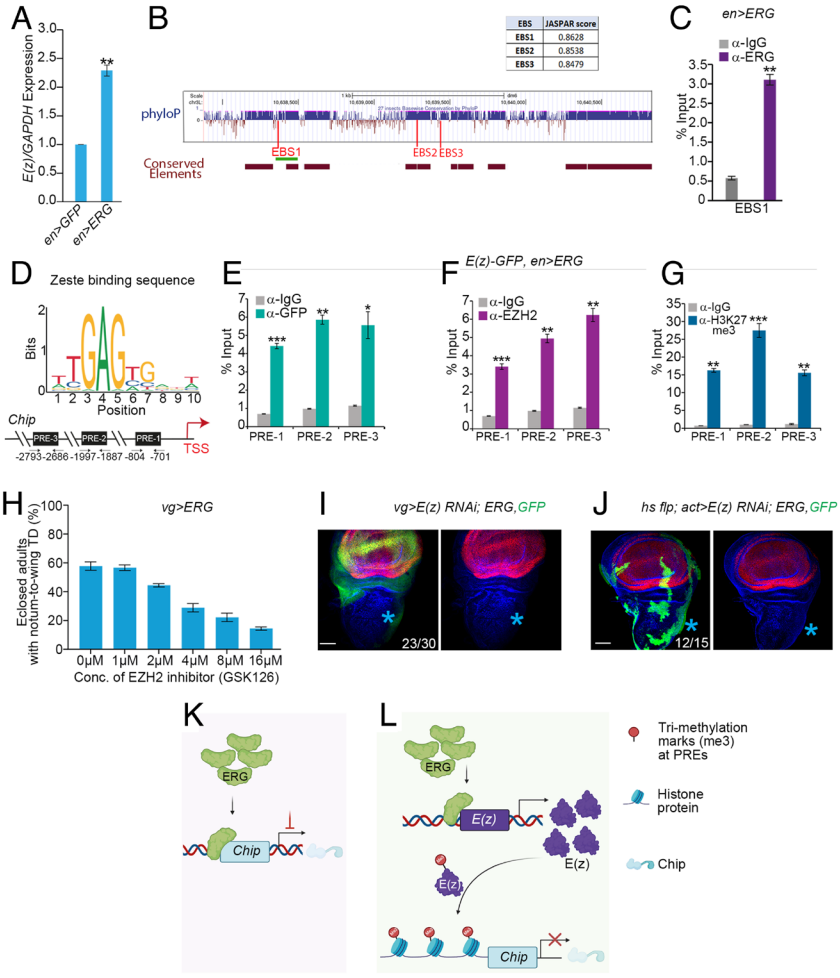

Fig. 5. ERG-up-regulated E(z) epigenetically represses *Chip*. (*A*) Quantification *E(z)* RNA (RT-qPCR) in *en>ERG* wing imaginal discs; RNA fold changes are expressed relative to that of its internal control, *GAPDH*. $^{**}P < 0.005$. (*B*) A schematic representation of evolutionarily conserved −3.0kb sequence upstream of *E(z)* TSS across 27 insect species using phyloP (see Fig. 3). Approximate positions of the predicted ERG/Ets21C-binding sites (EBSs) are marked by three vertical bars (red), while the bottom horizontal bars (brown) displayed highly conserved elements calculated by phastCons. The horizontal green line marks the region, which was further tested for physical binding of ERG by ChIP-qPCR. Inset table displays individual conservation scores of these three EBSs, as generated by JASPAR. (*C*) Enrichment of ERG binding to EBS1 assayed by ChIP-qPCR from *en>ERG* wing imaginal discs using an anti-ERG antibody. $^{**}P < 0.001$. (*D–G*) Consensus Zeste-binding sequence (*Top*, *D*) within a −3.0kb *Chip* TSS displays three Polycomb response elements, PREs (PRE1, PRE2, and PRE3, *Bottom*, *D*). Enrichment of these PREs in ChIP-qPCR from *E(z)-GFP*; *en>ERG* wing imaginal discs following pulled down with anti-GFP (*E*), mammalian anti-EZH2 (*F*), or anti-H3K27me3 (*G*). $^{*}P < 0.01$, $^{**}P < 0.001$, $^{***}P < 0.0001$. (*H*) Larvae (*vg>ERG*) fed on increasing concentrations of EZH2 inhibitor, GSK126, progressively displayed suppression of ERG-induced notum-to-wing transdetermination (TD) in eclosed adults. (*I* and *J*) Knockdown of *E(z)* in ERG-expressing wing imaginal discs (green, *vg>E(z) RNAi; ERG, GFP*, *I*) or in somatic clones (green, *hs flp; act>E(z) RNAi; ERG, GFP*, *J*) suppressed notum-to-wing transdetermination (blue star, *I′* and *J′*). (*K* and *L*) Schema displaying ERG-mediated suppression of *Chip* by its direct binding (*K*) and indirectly via E(z) (*L*). Scale bar, 50 μm; N= number of clones with the desired genotype scored in the notum /total number of wing discs observed.)

EBS1 through ChIP from *en>ERG* imaginal discs using ERG antibody (Fig. 5*C*).

E(z) is a transcriptional repressor, a core component of the Polycomb repressive complex 2, PRC2, which binds to the PREs of its targets [see refs. 72 and 73 and *SI Appendix, Methods*]. ERG-induced *E(z)* upregulation may thus contribute to the repression of ERG targets, such as *Chip*. Indeed, we noticed three PREs within the -3.0 kb CRM of *Chip* (Fig. 5*D*) that also harbored the EBSs (see Fig. 3*P*). These PREs were enriched in the ChIP of ERG-expressing wing imaginal discs [*E(z)-GFP*, *en>ERG*, Fig. 5 *E* and *F*] and displayed the trimethylation of lysine 27 on histone H3, H3K27me3 (Fig. 5*G*), a hallmark of E(z)-mediated epigenetic silencing (73).

The preceding observations thus suggest an E(z)-mediated silencing of *Chip* in ERG-expressing imaginal discs. To further test this interpretation, we fed *vg>ERG* larvae on food supplemented with a well-characterized inhibitor of EZH2, GSK126 (74). These animals display a progressive, concentration-dependent suppression of notum-to-wing transdetermination in *vg>ERG* animals (Fig. 5*H*). Likewise, a knockdown of *E(z)* in ERG-expressing notal epithelium (Fig. 5 *I* and *J*) extinguished notum-to-wing transdetermination. Thus, ERG directly represses *Chip* (Fig. 5*K*) on the one hand, and on the other, its upregulation of E(z) leads to epigenetic silencing of the former (Fig. 5*L*).

ERG-Induced Disruption of the Chip–Tup Complex Underpins Its Lineage-Specific Cooperative Carcinogenesis. *Drosophila* displays a well-known two-hit (75, 76) paradigm of cooperative carcinogenesis (76) in select developmental lineages (77–79). In cells displaying loss of a tumor suppressor, like Lgl, tumor progression is often driven via the recruitment of endogenously active signaling pathways (78). Given these developmental underpinnings of cooperative carcinogenesis, we reasoned that ERG gain might display lineage-restricted tumor cooperation in the posterior notum. Indeed, in the posterior notum, *lgl⁻; ERG⁺* clones displayed Nub expression (star, Fig. 6*A*)—reminiscent of that seen upon ERG gain in the posterior notum (see Fig. 2 *B* and *B′*). Further, *lgl⁻; ERG⁺* somatic clones displayed synthesis and secretion of Wg (Fig. 6 *B* and *B′*)—reminiscent of morphogen-sending neoplastic clones (80, 81)— besides inducing non-cell-autonomous hyperproliferation in the tumor microenvironment (arrow, PH3, red, Fig. 6 *C* and *D*). In the rest of the mosaic wing imaginal disc, *lgl⁻; ERG⁺* clones largely failed to display neoplastic transformation (white arrowheads, Fig. 6 *A–C*). Notably, a gain of N signaling in *lgl* clones, too, induced notum-to-wing cell fate switch and neoplastic transformation in the posterior notum (*lgl⁻; N^{intra}*, *SI Appendix*, Fig. S6 *A* and *B*) phenocopying their *lgl⁻; ERG⁺* counterpart (Fig. 6*A*). Finally, we note that *Chip* gain (Fig. 6 *E* and *E′*), *E(z)* knockdown (Fig. 6 *F* and *F′*), or sequestration of the Wg ligand (Fig. 6 *G* and *G′*) in *lgl⁻; ERG⁺* clones arrested their neoplastic transformation (white arrowheads, Fig. 6 *E′–G′*). Comparable results were also obtained by feeding host larvae with *lgl⁻; ERG⁺* mosaic discs on food supplemented with an *E(z)* inhibitor, GSK126 (white arrowheads, Fig. 6 *H* and *H′*).

Together, these results reveal that an ERG-induced, lineage-specific, cooperative carcinogenesis stems from its downregulation of *Chip*, leading to loss of Chip–Tup, LIM–HD complex, triggering an out-of-context N-mediated Wg signaling (Fig. 6*I*).

Prostate Cancer Cells Display ERG-Induced *LDB1* Repression. We noticed that a protein–protein interaction map centered on the Chip–Tup complex of *Drosophila* was comparable with its mammalian counterparts (*SI Appendix*, Fig. S7*A* and also see

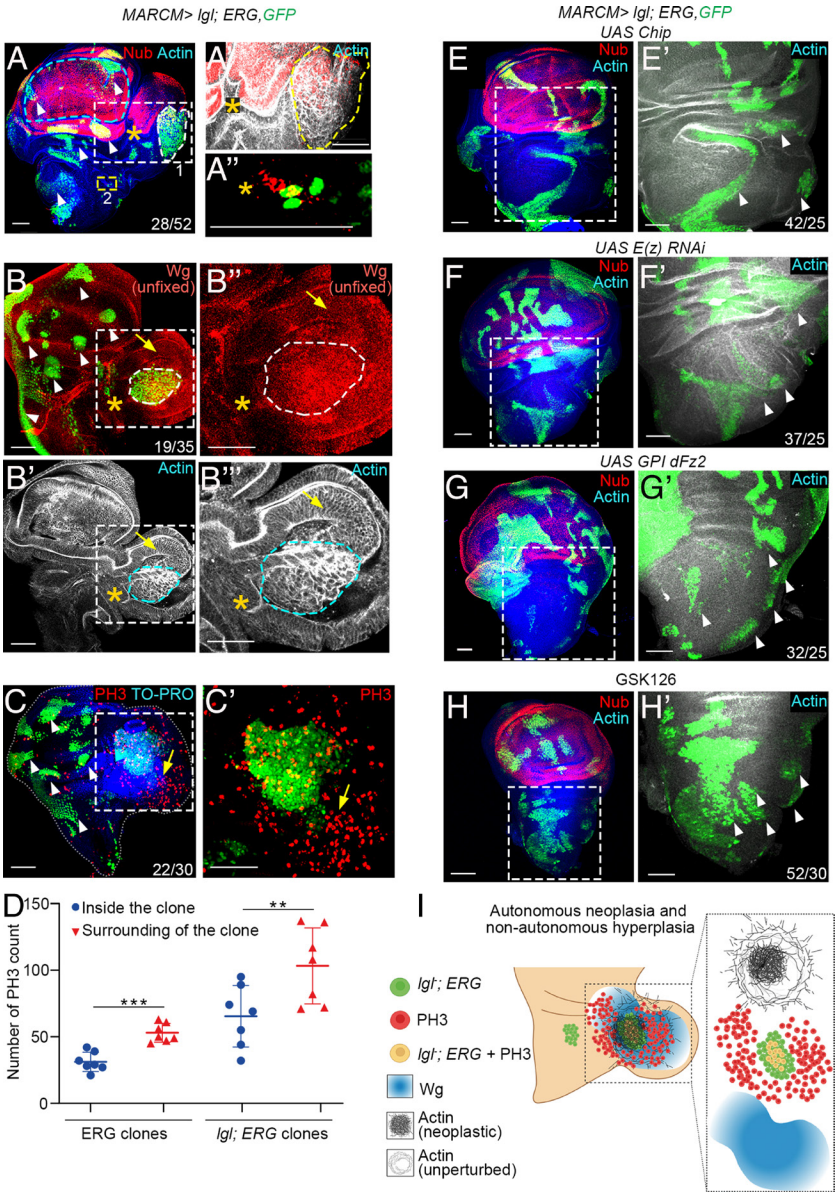

Fig. 6. ERG selectively cooperates for *lgl* tumorigenesis in the posterior notum. (*A–A″*) A mosaic wing imaginal disc displaying ERG-expressing *lgl*$^-$ somatic clones (*lgl*$^-$, *ERG*$^+$; *GFP*, green, *A*). Box 1 and box 2, respectively, mark a large and a small *lgl*$^-$, *ERG*$^+$ clone, which are displayed at higher magnifications in the right panels in (*A′*) and (*A″*). Endogenous wing (pouch) primordium is marked by broken blue line (*A*). Note the induction of non-cell autonomous notum-to-wing transdetermination in cells (only Nub-expressing, red, star, *A′*) overlapping with the clones (yellow, *A′*). The larger neoplastic transformation *lgl*$^-$, *ERG*$^+$ clonal area is marked (actin, broken yellow line, *A* and *A′*). Non-cell-autonomous growth and notum-to-wing transdetermination are marked by excessive epithelial folds and Nub expression (star, *A* and *A′*). The small clone in box 2 reveals, too, displays these essential hallmarks *lgl*$^-$, *ERG*$^+$ clone (*A* and *A″*). (*B–B‴*) An unfixed mosaic wing imaginal disc epithelium displaying *lgl*$^-$, *ERG*$^+$ clones (GFP, green) displaying secreted Wg (red). Boxed areas in (*B* and *B′*) are shown at higher magnification in their respective right panels (*B″* and *B‴*). Note the autonomous neoplasia within the clone (broken line, actin) while the surrounding epithelium display secreted Wg (arrow, *B′*) and hyperplasia, the latter marked by excessive epithelial foldings (arrow, *B–B‴*). *lgl*$^-$, *ERG*$^+$ clones induced in domains other than posterior notum did not display neoplastic transformation (white arrowheads, *B*). (*C* and *C′*) A mosaic wing imaginal disc epithelium with *lgl*$^-$*; ERG*$^+$clones (green), stained for a cell proliferation marker phospho-histone, PH3 (red). Boxed area in (*C*) is shown at higher magnification in (*C′*). Note the exaggerated PH3 uptake (arrow) around this transformed *lgl*$^-$*; ERG*$^+$clone in the posterior notum (arrow, green, *C′*) unlike their counterparts elsewhere (white arrowhead, *C*). (*D*) Quantification of cell-autonomous versus non-cell-autonomous PH3 uptake in *lgl*$^-$*; ERG*$^+$ clones as compared with their ERG-expressing control (see *SI Appendix, Methods*). **P* < 0.01. (*E–H*) *lgl*$^-$*; ERG*$^+$ clones in mosaic wing imaginal disc epithelia displaying simultaneous gain of *Chip* (*E*), knockdown of *E(z)* (*F*), expression of *GPI-dFz2*, membrane-tethered Wg receptor (*G*), or those from larvae fed on EZH2 inhibitor, GSK126 (25 mg/ml) (*H*). These *lgl*$^-$*; ERG*$^+$ clones neither induced Nub expression in posterior notum (*E–H*) nor displayed neoplasia (actin, white arrowheads, *E′–H′*). (*I*) Cartoon representation of selective carcinogenesis of *lgl*$^-$*; ERG*$^+$ somatic clones in the posterior notum (*I*). Scale bar, 50 μm. N= number of clones with the desired genotype scored in the notum /total number of wing discs observed.

ref. 82, (83), suggesting its ancient origin. We thus further asked if ERG targets the *LDB* genes, the mammalian homologs of *Drosophila Chip*; namely, LDB1 and LDB2, its two isoforms (84). *ERG* transcription and protein levels are minimal or absent in the healthy prostatic epithelium, whereas LDB1 and LDB2 show robust levels (*SI Appendix*, Fig. S7 *B–G*). Thus, we reasoned that ERG gain might target the repression of these *LDB*s. We chose to test this hypothesis in ERG-positive or -negative PCa cell lines. ChIP-Seq data of ERG-positive VCaP cell line [GSE28950, (84)] revealed binding peaks of ERG on the *LDB1* promoter (Fig. 7*A*) but not on that of *LDB2* (Fig. 7*B*). This binding peak was no longer seen in ChIP-Seq data of the VCaP cell line that displays knockdown of *ERG* [Fig. 7*C*, (GSE110655)]. We further noted the presence of a putative ERG-binding site (EBS) on the *LDB1* promoter (Fig. 7*D*), reminiscent of that seen in its *Drosophila* counterpart, *Chip* (see Fig. 3*P*). In agreement, in ChIP-qPCR using ERG-positive VCaP cells, we noticed the binding of ERG on the *LDB1* promoter (ERG_*LDB1* Fig. 7 *E* and *F*), suggesting a possible causal underpinning of transcriptional downregulation of the latter in this cell line. Conversely, a knockdown of ERG in the VCaP cells up-regulated *LDB1* expression (Fig. 7*G*). Gene expression data of an ERG-negative benign RWPE-1 prostate cell line revealed *LDB1* downregulation upon the gain of ERG (Fig. 7*H*). In contrast, gene expression data of an ERG-positive VCaP cells, *ERG*-knockdown up-regulated *LDB1* expression (Fig. 7*I*), further reconfirming an inverse association between *ERG* and *LDB1*. Finally, we also noticed the downregulation of *EZH2* upon ERG-knockdown in ERG-positive VCaP cells (Fig. 7*J*). Thus, *EZH2* is a transcriptional target of ERG in mammalian cancers (19, 84) reminiscent of that seen in *Drosophila* epithelium (Fig. 4). Together, these results reveal that ERG targets identified from *Drosophila* are conserved and functionally relevant for ERG-driven carcinogenesis in human.

Discussion

Identification of Human Oncoprotein Targets in *Drosophila* and Unraveling of Essential Cancer Mechanisms. Our results show that heterologous ERG oncoprotein targets repression of *Drosophila Chip*. One of the most striking fallouts of ERG gain is registered in the developing posterior notum of the wing imaginal disc, wherein disruption of Chip–Tup, LIM–HD complex leads to out-of-context N-Wg signaling. That ERG could be a transcriptional repressor of *Chip/LDB1* was not predictable from the large body of literature directed at identifying ERG targets in diverse cancers [for reviews, see refs. 25 and 85]. Moreover, although we could identify EBS on human *LDB1* promoter from

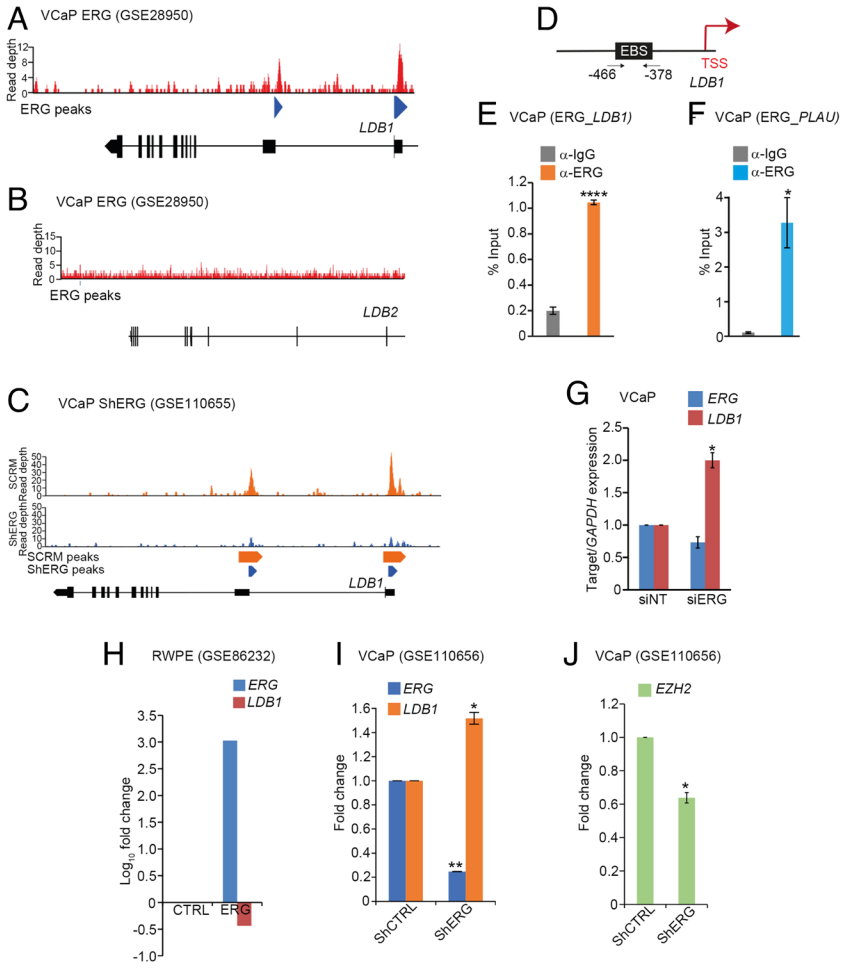

Fig. 7. ERG-positive VCaP PCa cells displays suppression of *LDB1*, a homolog of the *Drosophila Chip*. (*A* and *B*) ChIP-seq dataset of ERG-positive VCaP (GSE28950) reveals strong binding peaks (blue arrowhead MACS, Model-based Analysis of ChIP-seq) of ERG on *LDB1* (*A*), which are missing in *LDB2* (*B*). Below in black is the representation of *LDB1* and *LDB2* genes, wherein each vertical bar represents an exon. (*C*) ChIP-seq dataset of an ERG-positive VCaP (GSE110655) displays loss of ERG-binding peaks on *LDB1* upon knockdown of ERG (blue, *Bottom*) compared with control (orange, *Top*). Note orange arrowheads mark the ERG-binding MACS peak in control while reduced blue arrowheads display loss of ERG occupancy on *LDB1* upon ERG knockdown. (*D*) Coordinates of an ERG-binding site, EBS, on the *LDB1* locus, upstream of the TSS. (*E* and *F*) Enrichment of ERG at the predicted EBS in ChIP-qPCR of *LDB1* promoter (*E*); a known ERG target, *PLAU* (*Plasminogen activator urokinase*), served as an internal control (*F*). (*G*) Quantification of *LDB1* mRNA by qPCR following knockdown of *ERG* in VCaP cells. (*H*) Gene expression analysis in a benign prostate cell line (RWPE-1) displaying ERG over-expression (GSE86232) reveals downregulation of *LDB1*. (*I* and *J*) Gene expression analysis in ERG-positive VCaP displaying ERG knockdown (GSE110656). Note the upregulation of *LDB1* (*$P < 0.05$, *I*) while *EZH2* is down-regulated (**$P < 0.005$, *J*).

ChIP-seq data (Fig. 7) published previously (84), its relevance in cancer progression was not evident in the absence of a display of causal association. Finally, the shared consensus binding sequence of human ERG and fly Ets21C on the CRMs of *Chip* and *E(z)* reveal a rationale for discovering functionally relevant human oncoprotein targets in *Drosophila*. Given the deep homology of essential genetic tool kits of development, it is also not surprising that ERG-positive prostate cancer cells display suppression of *LDB1*, an ERG target revealed in *Drosophila*.

Our results further show that the spatial limits of expression of the LIM–HD complexes underlie lineage-specific ERG-induced carcinogenesis. By extension, the developmental history of an oncoprotein-targeted cell prefigures its propensities to become cancer cells-of-origin (see refs. 78 and 86). This essential principle of lineage-specific carcinogenesis may hold for cancers that entail disruption of the LIM–HD complexes. For instance, LDB1-mediated Wnt signaling appears to play a more significant role in proximal colorectal cancer than in distal (87). Likewise, different LIM–HD complex-dependent regulations of N and Wnt signaling could underpin cell-type specificity of ERG-induced cancers (16–18).

ERG Oncoprotein-Induced Pattern Formation in Transdetermined *Drosophila* Appendage. Our results show that ERG-induced Wg synthesis initially specifies wing cell fate-specification in the notum and subsequently drives its growth (33, 42, 44). Notably, de novo Wg (this study) or Dpp (81, 88) morphogen signaling centers thus drive tumor progression in cooperation with an oncogenic lesion. An ERG-induced Wg-signaling underlies its diverse, context-specific fallouts: cell fate switch alone or cell fate switch-linked tumor development in the posterior notum (Fig. 8). These findings reaffirm the maxim that carcinogenesis is essentially development gone awry (89, 90).

While the ERG-induced Wg in the posterior notum leads to amorphous wing tissue growth from the adult thorax (see Fig. 2), the shapes and sizes of some of these transdetermined wing primordia (Fig. 1) or the adult wings also suggest their acquisition of a near-perfect orthogonal positioning of AP (Dpp morphogen) and DV (Wg morphogen) signaling centers [Fig. 1 and see ref. 27]. We speculate that an initial non-cell-autonomous wing cell fate specification via secreted Wg from ERG-expressing cells of the posterior notum may underlie this phenomenon of near-perfect, albeit infrequent, positioning of morphogen-signaling centers. For instance, when a transdetermined wing primordium straddles an AP boundary (see Fig. 2*B*), the latter could provide the source of Dpp morphogen for a comprehensive wing patterning. A far more complex scenario may underlie the development of a Wg-morphogen-sending DV signaling center in a transdetermined wing primordia. For instance, since Ap expression is non-uniform in the notum (*SI Appendix*, Fig. S2), a non-cell-autonomous wing cell fate specification via secreted Wg may juxtapose domains of high and low Ap, reminiscent of that seen in the DV boundary of the endogenous wing (57). Alternatively, Wg signaling from a spatially aligned center in the posterior notum may be prefigured by an initial ERG-induced activation along polar coordinates of the transdetermined wing (42, 91). Further, Wg expression in the transdetermined wing may also display a feed-forward propagation of signals for its growth and patterning (29, 92).

A Future Strategy to Discover Oncogenic Networks in *Drosophila*. *Drosophila* provides unparalleled advantages in the genetic identification of tumor suppressors and oncogenes that control cellular functions ranging from maintenance of apicobasal polarity, chromatin architecture, and vesicular trafficking, to name a few (93). The genetic tractability of *Drosophila* has helped unravel elusive cancer mechanisms (78, 81, 94). *Drosophila* also displays the two-hit model of carcinogenesis seen in mammals (75, 76, 79). Further, modeling of human cancer in *Drosophila* is often based on a heterologous gain of an activated oncogene (95). Results presented here reveal an approach based on the deep homology of essential genetic tool kits and their crosstalks aided by the

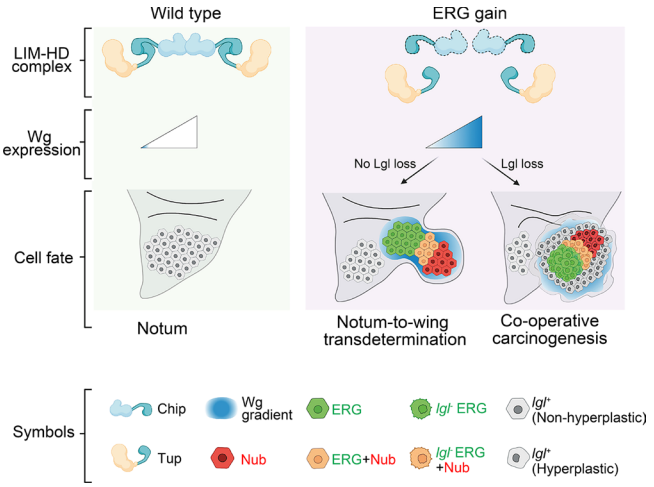

Fig. 8. ERG-induced disruption of Chip–Tup complex triggering Wg signaling display lineage-specific developmental and oncogenic fallouts. Schema of repression of Wg signaling by Chip–Tup, LIM–HD complex in the posterior notum (*Left*). ERG-induced suppression of *Chip* disrupts the Chip–Tup complex, activating Wg signaling that culminates in notum-to-wing transdetermination or, alternatively, neoplasia in collaboration with loss of Lgl tumor suppressor (*Right*) in a two-hit paradigm of carcinogenesis.

conservation of transcription factor-binding sites, like EBS shown here, on the oncoprotein targets. In turn, phenotypic fallouts of heterologous gain of an oncoprotein offer clues to its crosstalk with a diverse set of functionally relevant pathways that could double up as oncogenic signaling nodes. For instance, activation of Wg signaling in the notum was also reported earlier upon loss of Osa (32) or subunits of BAP (Brm-associated protein) (96), which are members of a highly conserved chromatin remodeling complex. Osa/BAP, therefore, could be part of the ERG signaling network. Indeed, the binding of ERG to the BAP/BAF chromatin remodeling complex has been reported in prostate cancer (97).

Materials and Methods

***Drosophila* Stocks, Transgenic Line, and Genetic Mosaic Studies.** *Drosophila stocks and method for generation of transgenic fly line and clones (78) are described in SI Appendix,* Table S1.

Immunohistochemistry. Method and antibodies are described in *SI Appendix*.

Chromatin Immunoprecipitaion and -qRT-PCR. ChIP was performed using LowCell# ChIP kit protein A (Diagenode, C01010072). For details, see *SI Appendix*. RNA was extracted using TRIZOL followed by cDNA synthesis (Invitrogen). Fold changes for individual genes was quantified using ΔΔCt method, with *GAPDH* as internal control. Primer details in *SI Appendix*, Table S2.

ChIP-seq analysis. Publicly available ChIP-Seq data (GSE28950, GSE116055) were used to determine the recruitment of ERG on *LDB1* and *LDB2* promoter. For details, see *SI Appendix*.

Prediction of Transcription Factor binding and evolutionary conservation. JASPAR was used to look for putative Ets21C/ERG binding sites (EBSs) in *E(z)* and *Chip* promoter, and PREs, in the *Chip* promoter (for further details, see *SI Appendix*). *Evolutionary conservation of Ets21C/ERG binding on Chip and E(z) upstream regulatory sequence was done using PHAST package at the USCS genome browser.* Further details are presented in *SI Appendix*.

Gene Expression Analysis. Datasets (GSE86232, GSE110656) were analyzed for *LDB1* expression. For detail, see *SI Appendix*.

Data, Materials, and Software Availability. Contact Pradip Sinha (pradips@iitk.ac.in) for transgenic fly line generated in this study. We have used published data (GSE28950, GSE110655, GSE86232) and did not generate any shared data.

ACKNOWLEDGMENTS. We thank Martin Müller of the University of Zurich for the gift of Ap antibody. This work was supported by Science & Engineering Research Board (SERB), Department of Science and Technology (New Delhi) research grant no. EMR/2016/006723 to P.S. and B.A. M.B and N.M. were supported by University Grants Commission (New Delhi). A.B. was supported by an Early career fellowship by DBT Wellcome Trust India Alliance (IA/E/13/1/501271). B.A. is a Senior Fellow of the DBT/ Wellcome Trust India Alliance and acknowledges financial support from the DBT/Wellcome Trust India Alliance (Grant Number: IA/S/19/2/504659); SERB-POWER (Grant Number: SPG/2021/000851) and S. Ramachandran-National Bioscience Award for Career Development (Grant Number: BT/HRD/NBA/NWB/39/2020–21) from the Department of Biotechnology. B. A and P. S. are respectively, co- and lead-corresponding authors of this paper.

Author affiliations: [a]Biological Sciences and Bioengineering, Indian Institute of Technology Kanpur, India, 208016; [b]Mehta Family Center for Engineering in Medicine, Indian Institute of Technology Kanpur, India, 208016; and [c]National Institute of Immunology, India, 110067

1. N. Shubin, C. Tabin, S. Carroll, Deep homology and the origins of evolutionary novelty. *Nature* **457**, 818–823 (2009).
2. C. Larroux *et al.*, Genesis and expansion of metazoan transcription factor gene classes. *Mol. Biol. Evol.* **25**, 980–996 (2008).
3. I. Bach, The LIM domain: Regulation by association. *Mech. Dev.* **91**, 5–17 (2000).
4. D. J. van Meyel *et al.*, Chip and Apterous physically interact to form a functional complex during *Drosophila* development. *Mol. Cell* **4**, 259–265 (1999).
5. M. Milán, S. M. Cohen, Regulation of LIM homeodomain activity *in vivo*: A tetramer of dLDB and Apterous confers activity and capacity for regulation by dLMO. *Mol. Cell* **4**, 267–273 (1999).
6. R. Bronstein, D. Segal, Modularity of CHIP/LDB transcription complexes regulates cell differentiation. *Fly (Austin)* **5**, 200–205 (2011).
7. L. W. Jurata, G. N. Gill, "LIM domain genes" in *Encyclopedia of Genetics*, S. Brenner, J. H. Miller, Eds. (Academic Press, 2001), pp. 1096–1099.
8. Y. Kawakami *et al.*, Islet1-mediated activation of the β-catenin pathway is necessary for hindlimb initiation in mice. *Development* **138**, 4465–4473 (2011).
9. G. Narkis *et al.*, Isl1 and Ldb co-regulators of transcription are essential early determinants of mouse limb development. *Dev. Dyn.* **241**, 787–791 (2012).
10. A. A. Mohamed *et al.*, Ets family protein, ERG expression in developing and adult mouse tissues by a highly specific monoclonal antibody. *J. Cancer* **1**, 197–208 (2010).
11. V. Vlaeminck-Guillem *et al.*, The Ets family member *ERG* gene is expressed in mesodermal tissues and neural crests at fundamental steps during mouse embryogenesis. *Mech. Dev.* **91**, 331–335 (2000).
12. S. A. Tomlins, N. Palanisamy, J. Siddiqui, A. M. Chinnaiyan, L. P. Kunju, Antibody-based detection of ERG rearrangements in prostate core biopsies, including diagnostically challenging cases: ERG staining in prostate core biopsies. *Arch. Pathol. Lab. Med.* **136**, 935–946 (2012).
13. S. A. Tomlins *et al.*, Recurrent Fusion of TMPRSS2 and ETS transcription factor genes in prostate cancer. *Science* **310**, 644–648 (2005).
14. Cancer Genome Atlas Research Network, The molecular taxonomy of primary prostate cancer. *Cell* **163**, 1011–1025 (2015).
15. T. G. P. Grünewald *et al.*, Ewing sarcoma. *Nat. Rev. Dis. Primer* **4**, 5 (2018).
16. S. Tsuzuki, O. Taguchi, M. Seto, Promotion and maintenance of leukemia by ERG. *Blood* **117**, 3858–3868 (2011).
17. K. J. Kron *et al.*, TMPRSS2-ERG fusion co-opts master transcription factors and activates NOTCH signaling in primary prostate cancer. *Nat. Genet.* **49**, 1336–1345 (2017).
18. L. Wu *et al.*, ERG is a critical regulator of Wnt/LEF1 signaling in prostate cancer. *Cancer Res.* **73**, 6068–6079 (2013).
19. J. Yu *et al.*, An integrated network of androgen receptor, polycomb, and TMPRSS2-ERG gene fusions in prostate cancer progression. *Cancer Cell* **17**, 443–454 (2010).
20. S. Goel *et al.*, Transcriptional network involving ERG and AR orchestrates Distal-less homeobox-1 mediated prostate cancer progression. *Nat. Commun.* **12**, 5325 (2021).
21. A. H. Davies, H. Beltran, A. Zoubeidi, Cellular plasticity and the neuroendocrine phenotype in prostate cancer. *Nat. Rev. Urol.* **15**, 271–286 (2018).
22. J. Malicki, K. Schughart, W. McGinnis, Mouse Hox-2.2 specifies thoracic segmental identity in *Drosophila* embryos and larvae. *Cell* **63**, 961–967 (1990).
23. G. Halder, P. Callaerts, W. J. Gehring, Induction of ectopic eyes by targeted expression of the *eyeless* gene in *Drosophila*. *Science* **267**, 1788–1792 (1995).
24. J. A. Lautenberger *et al.*, Genomic dispersal of the *ETS* gene family during metazoan evolution. *Oncogene* **7**, 1713–1719 (1992).
25. P. C. Hollenhorst, L. P. McIntosh, B. J. Graves, Genomic and biochemical insights into the specificity of ETS transcription factors. *Annu. Rev. Biochem.* **80**, 437–471 (2011).
26. B. Cohen, A. A. Simcox, S. M. Cohen, Allocation of the thoracic imaginal primordia in the *Drosophila* embryo. *Development* **117**, 597–608 (1993).
27. L. Barrio, M. Milán, Regulation of anisotropic tissue growth by two orthogonal signaling centers. *Dev. Cell* **52**, 659–672.e3 (2020).
28. J. Parker, G. Struhl, Control of *Drosophila* wing size by morphogen range and hormonal gating. *Proc. Natl. Acad. Sci. U.S.A.* **117**, 31935–31944 (2020).
29. M. Zecca, G. Struhl, A unified mechanism for the control of *Drosophila* wing growth by the morphogens Decapentaplegic and Wingless. *PLoS Biol.* **19**, e3001111 (2021).

30. M. Ng, F. J. Diaz-Benjumea, S. M. Cohen, Nubbin encodes a POU-domain protein required for proximal-distal patterning in the *Drosophila* wing. *Development* **121**, 589–599 (1995).
31. J. D. Zirin, R. S. Mann, Nubbin and Teashirt mark barriers to clonal growth along the proximal–distal axis of the *Drosophila* wing. *Dev. Biol.* **304**, 745–758 (2007).
32. R. T. Collins, J. E. Treisman, Osa-containing Brahma chromatin remodeling complexes are required for the repression of *wingless* target genes. *Genes Dev.* **14**, 3140–3152 (2000).
33. M. Ng, F. J. Diaz-Benjumea, J.-P. Vincent, J. Wu, S. M. Cohen, Specification of the wing by localized expression of Wingless protein. *Nature* **381**, 316–318 (1996).
34. S. D. Weatherbee, G. Halder, J. Kim, A. Hudson, S. Carroll, Ultrabithorax regulates genes at several levels of the wing-patterning hierarchy to shape the development of the *Drosophila* haltere. *Genes Dev.* **12**, 1474–1482 (1998).
35. A. J. Simmonds, W. J. Brook, S. M. Cohen, J. B. Bell, Distinguishable functions for *engrailed* and *invected* in anterior-posterior patterning in the *Drosophila* wing. *Nature* **376**, 424–427 (1995).
36. J. A. Williams, S. W. Paddock, K. Vorwerk, S. B. Carroll, Organization of wing formation and induction of a wing-patterning gene at the dorsal/ventral compartment boundary. *Nature* **368**, 299–305 (1994).
37. C. Schwartz, J. Locke, C. Nishida, T. B. Kornberg, Analysis of *cubitus interruptus* regulation in *Drosophila* embryos and imaginal discs. *Development* **121**, 1625–1635 (1995).
38. T. Lecuit *et al.*, Two distinct mechanisms for long-range patterning by Decapentaplegic in the *Drosophila* wing. *Nature* **381**, 387–393 (1996).
39. M. I. Worley, L. Setiawan, I. K. Hariharan, Regeneration and transdetermination in *Drosophila* imaginal discs. *Annu. Rev. Genet.* **46**, 289–310 (2012).
40. M. Schubiger, A. Sustar, G. Schubiger, Regeneration and transdetermination: The role of *wingless* and its regulation. *Dev. Biol.* **347**, 315–324 (2010).
41. C. L. Salzer, J. P. Kumar, Identification of retinal transformation hot spots in developing *Drosophila* epithelia. *PloS One* **5**, e8510 (2010).
42. J. P. Couso, M. Bate, A. Martínez-Arias, A *wingless*-dependent polar coordinate system in *Drosophila* imaginal discs. *Science* **259**, 484–489 (1993).
43. J. Kim *et al.*, Integration of positional signals and regulation of wing formation and identity by *Drosophila vestigial* gene. *Nature* **382**, 133–138 (1996).
44. E. Gracia-Latorre, L. Pérez, M. Muzzopappa, M. Milán, A single WNT enhancer drives specification and regeneration of the *Drosophila* wing. *Nat. Commun.* **13**, 4794 (2022).
45. F. J. Diaz-Benjumea, S. M. Cohen, Serrate signals through Notch to establish a Wingless-dependent organizer at the dorsal/ventral compartment boundary of the *Drosophila* wing. *Dev. Camb. Engl.* **121**, 4215–4225 (1995).
46. A. J. Giraldez, S. M. Cohen, Wingless and Notch signaling provide cell survival cues and control cell proliferation during wing development. *Development* **130**, 6533–6543 (2003).
47. G. Struhl, K. Fitzgerald, I. Greenwald, Intrinsic activity of the Lin-12 and Notch intracellular domains *in vivo*. *Cell* **74**, 331–345 (1993).
48. I. Rebay, R. G. Fehon, S. Artavanis-Tsakonas, Specific truncations of *Drosophila* Notch define dominant activated and dominant negative forms of the receptor. *Cell* **74**, 319–329 (1993).
49. W. Helms *et al.*, Engineered truncations in the *Drosophila* mastermind protein disrupt Notch pathway function. *Dev. Biol.* **215**, 358–374 (1999).
50. K. M. Cadigan, M. P. Fish, E. J. Rulifson, R. Nusse, Wingless repression of *Drosophila frizzled 2* expression shapes the Wingless morphogen gradient in the wing. *Cell* **93**, 767–777 (1998).
51. G. Struhl, K. Basler, Organizing activity of Wingless protein in *Drosophila*. *Cell* **72**, 527–540 (1993).
52. J. de Navascués, J. Modolell, *tailup*, a LIM-HD gene, and *Iro-C* cooperate in *Drosophila* dorsal mesothorax specification. *Development* **134**, 1779–1788 (2007).
53. J.-Y. Roignant, K. Legent, F. Janody, J. E. Treisman, The transcriptional co-factor Chip acts with LIM-homeodomain proteins to set the boundary of the eye field in *Drosophila*. *Development* **137**, 273–281 (2010).
54. I. Biryukova, P. Heitzler, The *Drosophila* LIM-homeo domain protein Islet antagonizes pro-neural cell specification in the peripheral nervous system. *Dev. Biol.* **288**, 559–570 (2005).
55. E. Torigoi *et al.*, Chip interacts with diverse homeodomain proteins and potentiates Bicoid activity *in vivo*. *Proc. Natl. Acad. Sci. U. S. A.* **97**, 2686–2691 (2000).
56. J. A. Castro-Mondragon *et al.*, JASPAR 2022: The 9th release of the open-access database of transcription factor binding profiles. *Nucleic Acids Res.* **50**, D165–D173 (2022).
57. F. J. Diaz-Benjumea, S. M. Cohen, Interaction between dorsal and ventral cells in the imaginal disc directs wing development in *Drosophila*. *Cell* **75**, 741–752 (1993).
58. B. Cohen, M. E. McGuffin, C. Pfeifle, D. Segal, S. M. Cohen, *apterous*, a gene required for imaginal disc development in *Drosophila* encodes a member of the LIM family of developmental regulatory proteins. *Genes Dev.* **6**, 715–729 (1992).
59. M. Milán, S. M. Cohen, Temporal regulation of Apterous activity during development of the *Drosophila* wing. *Development* **127**, 3069–3078 (2000).
60. T. Chen, M. Bunting, F. D. Karim, C. S. Thummel, Isolation and characterization of five *Drosophila* genes that encode an ETS-related DNA binding domain. *Dev. Biol.* **151**, 176–191 (1992).
61. T. Hsu, R. A. Schulz, Sequence and functional properties of *ETS* genes in the model organism *Drosophila*. *Oncogene* **19**, 6409–6416 (2000).
62. E. Külshammer *et al.*, Interplay among *Drosophila* transcription factors Ets21c, Fos and Ftz-F1 drives JNK-mediated tumor malignancy. *Dis. Model. Mech.* **8**, 1279–1293 (2015).
63. J. Toggweiler, M. Willecke, K. Basler, The transcription factor Ets21C drives tumor growth by cooperating with AP-1. *Sci. Rep.* **6**, 1–10 (2016).
64. J. Mundorf, C. D. Donohoe, C. D. McClure, T. D. Southall, M. Uhlirova, Ets21C governs tissue renewal, stress tolerance, and aging in the *Drosophila* intestine. *Cell Rep.* **27**, 3019–3033.e5 (2019).
65. M. I. Worley *et al.*, Ets21C sustains a pro-regenerative transcriptional program in blastema cells of *Drosophila* imaginal discs. *Curr. Biol.* **32**, 3350–3364.e6 (2022).
66. R. A. Patterson *et al.*, Serine proteolytic pathway activation reveals an expanded ensemble of wound response genes in *Drosophila*. *PloS One* **8**, e61773 (2013).
67. O. M. Ahmed *et al.*, Evolution of mechanisms that control mating in *Drosophila* males. *Cell Rep.* **27**, 2527–2536.e4 (2019).
68. A. Siepel *et al.*, Evolutionarily conserved elements in vertebrate, insect, worm, and yeast genomes. *Genome Res.* **15**, 1034–1050 (2005).
69. P. Morcillo, C. Rosen, M. K. Baylies, D. Dorsett, Chip, a widely expressed chromosomal protein required for segmentation and activity of a remote wing margin enhancer in *Drosophila*. *Genes Dev.* **11**, 2729–2740 (1997).
70. K. H. Kim, C. W. M. Roberts, Targeting EZH2 in cancer. *Nat. Med.* **22**, 128–134 (2016).
71. L. Ringrose, R. Paro, Epigenetic regulation of cellular memory by the Polycomb and Trithorax group proteins. *Annu. Rev. Genet.* **38**, 413–443 (2004).
72. L. Ringrose, M. Rehmsmeier, J.-M. Dura, R. Paro, Genome-wide prediction of Polycomb/Trithorax response elements in *Drosophila melanogaster*. *Dev. Cell* **5**, 759–771 (2003).
73. B. Schuettengruber, D. Chourrout, M. Vervoort, B. Leblanc, G. Cavalli, Genome regulation by Polycomb and Trithorax proteins. *Cell* **128**, 735–745 (2007).
74. J. Kim *et al.*, Polycomb- and methylation-independent roles of EZH2 as a transcription activator. *Cell Rep.* **25**, 2808–2820.e4 (2018).
75. R. A. Pagliarini, T. Xu, A genetic screen in *Drosophila* for metastatic behavior. *Science* **302**, 1227–1231 (2003).
76. A. M. Brumby, H. E. Richardson, Using *Drosophila melanogaster* to map human cancer pathways. *Nat. Rev. Cancer* **5**, 626–639 (2005).
77. R. P. Gupta, A. Bajpai, P. Sinha, Selector genes display tumor cooperation and inhibition in *Drosophila* epithelium in a developmental context-dependent manner. *Biol. Open* **6**, 1581–1591 (2017).
78. S. J. Khan *et al.*, Epithelial neoplasia in *Drosophila* entails switch to primitive cell states. *Proc. Natl. Acad. Sci. U.S.A.* **110**, E2163–2172 (2013).
79. J. Menéndez, A. Pérez-Garijo, M. Calleja, G. Morata, A tumor-suppressing mechanism in *Drosophila* involving cell competition and the Hippo pathway. *Proc. Natl. Acad. Sci. U.S.A.* **107**, 14651–14656 (2010).
80. J. C. D. Bairzin, M. Emmons-Bell, I. K. Hariharan, The Hippo pathway coactivator Yorkie can reprogram cell fates and create compartment-boundary-like interactions at clone margins. *Sci. Adv.* **6**, eabe8159 (2020).
81. A. Bajpai, P. Sinha, Hh signaling from *de novo* organizers drive *lgl* neoplasia in *Drosophila* epithelium. *Dev. Biol.* **457**, 1–8 (2020).
82. A. J. W. Te Velthuis, T. Isogai, L. Gerrits, C. P. Bagowski, Insights into the molecular evolution of the PDZ/LIM family and identification of a novel conserved protein motif. *PloS One* **2**, e189 (2007).
83. J. M. Matthews, J. E. Visvader, LIM-domain-binding protein 1: A multifunctional cofactor that interacts with diverse proteins. *EMBO Rep.* **4**, 1132–1137 (2003).
84. K. R. Chng *et al.*, A transcriptional repressor co-regulatory network governing androgen response in prostate cancers. *EMBO J.* **31**, 2810–2823 (2012).
85. X. Lin *et al.*, Signaling networks in TMPRSS2-ERG positive prostate cancers: Do we need a pied piper or sharpshooter to deal with "at large" fused oncoprotein. *Cell. Mol. Biol. Noisy–Gd. Fr.* **63**, 1–8 (2017).
86. J. E. Visvader, Cells of origin in cancer. *Nature* **469**, 314–322 (2011).
87. S. A. García *et al.*, *LDB1* overexpression is a negative prognostic factor in colorectal cancer. *Oncotarget* **7**, 84258–84270 (2016).
88. H. Herranz, R. Weng, S. M. Cohen, Crosstalk between epithelial and mesenchymal tissues in tumorigenesis and imaginal disc development. *Curr. Biol. CB* **24**, 1476–1484 (2014).
89. M. Berdasco, M. Esteller, Aberrant epigenetic landscape in cancer: How cellular identity goes awry. *Dev. Cell* **19**, 698–711 (2010).
90. A. M. Soto, M. V. Maffini, C. Sonnenschein, Neoplasia as development gone awry: The role of endocrine disruptors. *Int. J. Androl.* **31**, 288–293 (2008).
91. V. French, P. J. Bryant, S. V. Bryant, Pattern regulation in epimorphic fields. *Science* **193**, 969–981 (1976).
92. M. Zecca, G. Struhl, A feed-forward circuit linking wingless, Fat-Dachsous signaling, and the Warts-Hippo pathway to *Drosophila* wing growth. *PLoS Biol.* **8**, e1000386 (2010).
93. D. Bilder, M. Li, N. Perrimon, Cooperative regulation of cell polarity and growth by *Drosophila* tumor suppressors. *Science* **289**, 113–116 (2000).
94. Y. Tamori, E. Suzuki, W.-M. Deng, Epithelial tumors originate in tumor hotspots, a tissue-intrinsic microenvironment. *PLoS Biol.* **14**, e1002537 (2016).
95. R. D. Read *et al.*, A *Drosophila* model of multiple endocrine neoplasia type 2. *Genetics* **171**, 1057–1081 (2005).
96. S. Song, H. Herranz, S. M. Cohen, The chromatin remodeling BAP complex limits tumor-promoting activity of the Hippo pathway effector Yki to prevent neoplastic transformation in *Drosophila* epithelia. *Dis. Model. Mech.* **10**, 1201–1209 (2017).
97. G. J. Sandoval *et al.*, Binding of TMPRSS2-ERG to BAF Chromatin remodeling complexes mediates prostate oncogenesis. *Mol. Cell* **71**, 554–566.e7 (2018).